Paracellin-1, a Renal Tight Junction Protein Required for Paracellular Mg^{2+} Resorption

David B. Simon,[1,2]* Yin Lu,[1,2]* Keith A. Choate,[1,2] Heino Velazquez,[2] Essam Al-Sabban,[3] Manuel Praga,[4] Giorgio Casari,[5] Alberto Bettinelli,[6] Giacomo Colussi,[7] Juan Rodriguez-Soriano,[8] David McCredie,[9] David Milford,[10] Sami Sanjad,[11] Richard P. Lifton[1,2]†

Epithelia permit selective and regulated flux from apical to basolateral surfaces by transcellular passage through cells or paracellular flux between cells. Tight junctions constitute the barrier to paracellular conductance; however, little is known about the specific molecules that mediate paracellular permeabilities. Renal magnesium ion (Mg^{2+}) resorption occurs predominantly through a paracellular conductance in the thick ascending limb of Henle (TAL). Here, positional cloning has identified a human gene, *paracellin-1* (*PCLN-1*), mutations in which cause renal Mg^{2+} wasting. PCLN-1 is located in tight junctions of the TAL and is related to the claudin family of tight junction proteins. These findings provide insight into Mg^{2+} homeostasis, demonstrate the role of a tight junction protein in human disease, and identify an essential component of a selective paracellular conductance.

The composition of fluids on opposite sides of epithelial cell layers is often different, and is maintained by barriers to passage of fluid, electrolytes, nutrients, pathogens, and cells. Cellular membranes provide a transcellular barrier, whereas the tight junctions (*zonula occludens*) have long been recognized to constitute the intercellular permeability barrier (*1*). These transcellular and paracellular barriers are not absolute, and they often display selective and regulated conductances (*2*). Although many mediators of transcellular flux have been characterized, specific determinants of paracellular permeabilities are unknown. Several components of the tight junction have been identified at the molecular level (*3*), but their specific roles have yet to be determined.

Magnesium is a critical cofactor in a wide variety of biological activities. The renal resorption of Mg^{2+} occurs predominantly by paracellular flux (*4*) in the thick ascending limb of Henle (TAL) (*5*), a process driven by a favorable electrochemical gradient (Fig. 1A). The conductance of this paracellular pathway is highly regulated (*6*), with renal Mg^{2+} excretion varying from 0.5 to 80% of the filtered load with low or high serum Mg^{2+} concentrations, respectively (*7*). Interestingly, although this paracellular pathway shows relatively high magnesium conductance, it is highly impermeable to water (*8*).

With these observations in mind, a rare autosomal recessive disease, renal hypomagnesemia with hypercalciuria and nephrocalcinosis, is an intriguing entity (*9*). Affected persons have profound renal Mg^{2+} wasting, which results in severe hypomagnesemia that is not corrected by oral or intravenous Mg^{2+} supplementation. They also have renal Ca^{2+} wasting, resulting in renal parenchymal calcification and renal failure. Other features include urinary tract infections, kidney stones, hyperuricemia, and ocular findings. These patients do not display salt wasting, and renal transplantation cures the defects in electrolyte homeostasis. Because the massive renal Mg^{2+} loss suggests a defect in paracellular resorption, identification of the disease gene could provide insight into the nature of paracellular permeabilities and regulation of magnesium homeostasis.

Twelve kindreds with typical recessive renal hypomagnesemia were recruited for study (*10, 11*); in 10 families affected persons were the offspring of consanguineous unions. To map the gene (or genes) causing hypomagnesemia in these kindreds, we genotyped polymorphic loci across the human genome and analyzed linkage to the trait (*12*). Initial analysis of three consanguineous kindreds demonstrated linkage to a segment of chromosome 3q, with affected persons homozygous for many consecutive markers in this interval and a lod score (logarithm of odds ratio for linkage) of 6.8 (*11*). All other families also supported linkage to this segment, and two provided the basis for a refined location of the disease gene. In kindred K113, 11 distantly related affected members were studied (Fig. 1B). All showed homozygosity on 3q (estimated lod score, >20); however, all shared homozygosity for identical alleles of only two consecutive markers, *D3S1314* and *539-5* (Fig. 1C). Analysis of kindred K114, with two affected siblings from a second-cousin marriage, further refined the location of the trait locus, with one affected sibling losing homozygosity at locus *539*-5 (Fig. 1C). Together these findings localize the trait locus to the approximately 1-centimorgan interval flanked by loci *539-5* and *D3S1288*.

We next constructed a physical map of the interval by selection of bacterial artificial chromosome (BAC) clones hybridizing to sequence-tagged sites (STSs) and polymorphic markers from the critical interval (*13*). The results demonstrate a continuous map spanning about 1 Mb in genomic DNA (Fig. 1D). The flanking markers *539-5* and *D3S1288* are contained in the physical map and are separated by no more than 500 kb, which shows that the trait locus lies within this short chromosomal interval.

Examination of public databases revealed no known genes in the critical interval. Candidate genes were sought by exon trapping using BACs from the physical map (*14*). One of the resulting clones, trapped from BAC 1314-14, yielded a product containing a putative 54–amino acid open reading frame (ORF), which ultimately proved to be exon 3 of a gene. The complete ORF of this gene, which we have termed *paracellin-1* (*PCLN-1*), was determined (*14*) and sequence analysis showed that it encodes a protein of 305 amino acids (Fig. 2A) with four transmembrane domains and intracellular NH_2- and COOH-termini (*11, 15*). The PCLN-1 protein shows sequence and structural similarity to members of the claudin family (Fig. 2A) (*15, 16*) and is the most distantly related member of this family (Fig. 2B). More than a dozen members of this family have been identified; all localize to tight junctions and appear to bridge the intercellular space by homo- or heterotypic interactions (*17*). PCLN-1 shows 10 to 18% amino acid identity with individual claudins (*11*), with the highest homology in a segment of the first extracellular domain that is thought to bridge the intercellular space (*17*). In addi-

[1]Howard Hughes Medical Institute, Department of Genetics, [2]Department of Medicine, Yale University School of Medicine, New Haven, CT 06510, USA. [3]Department of Pediatrics, King Faisal Specialist Hospital and Research Center, Riyadh, Saudi Arabia. [4]Servicio de Nefrologia, Hospital 12 de Octubre, Madrid, Spain. [5]Telethon Institute of Genetics and Medicine, Milan 20132, Italy. [6]Department of Pediatrics II, University of Milan, Milan, Italy. [7]Renal Division, Niguarda "Ca' Granda" Hospital, Milan, Italy. [8]Department of Pediatrics, Hospital de Cruces, Baracaldo E-48903, Spain. [9]Department of Nephrology, Royal Children's Hospital, Flemington Road, Parkville, Victoria 3052, Australia. [10]Department of Nephrology, Birmingham Children's Hospital, Birmingham B16 8ET, UK. [11]Department of Pediatrics, American University, Beirut, Lebanon.

*These authors contributed equally to this report.
†To whom correspondence should be addressed. E-mail: richard.lifton@yale.edu

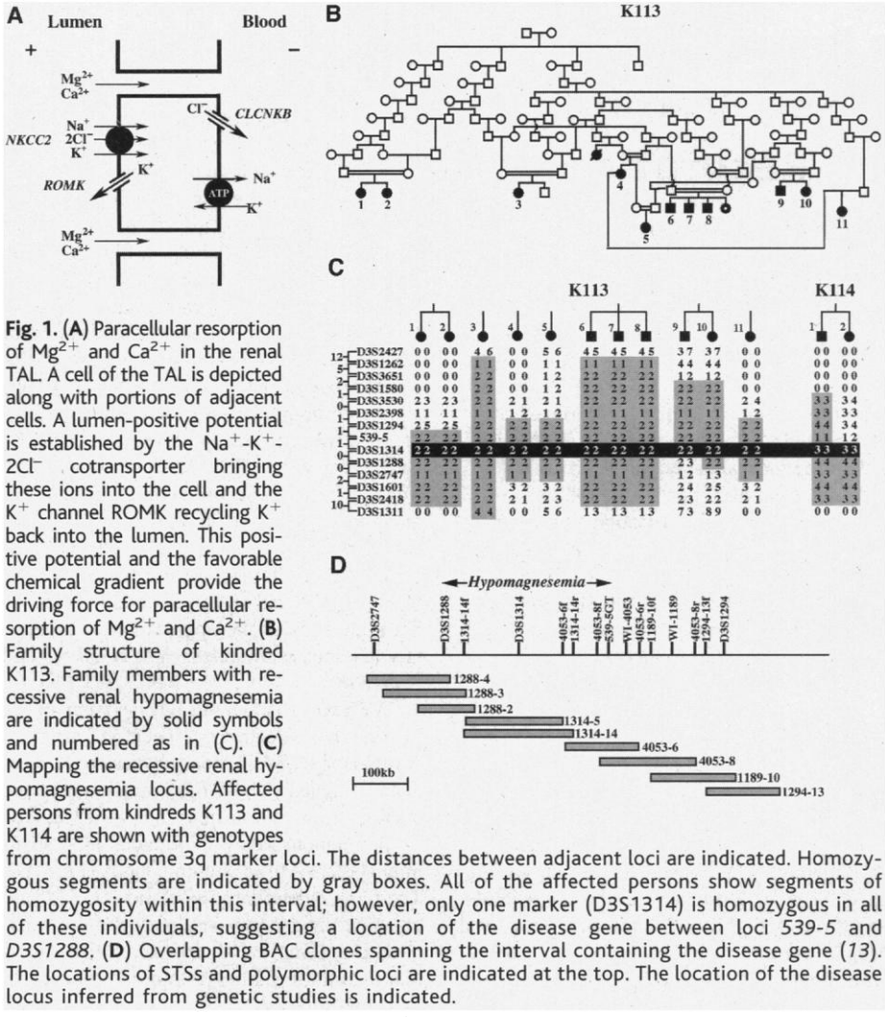

Fig. 1. (**A**) Paracellular resorption of Mg^{2+} and Ca^{2+} in the renal TAL. A cell of the TAL is depicted along with portions of adjacent cells. A lumen-positive potential is established by the Na^+-K^+-$2Cl^-$ cotransporter bringing these ions into the cell and the K^+ channel ROMK recycling K^+ back into the lumen. This positive potential and the favorable chemical gradient provide the driving force for paracellular resorption of Mg^{2+} and Ca^{2+}. (**B**) Family structure of kindred K113. Family members with recessive renal hypomagnesemia are indicated by solid symbols and numbered as in (C). (**C**) Mapping the recessive renal hypomagnesemia locus. Affected persons from kindreds K113 and K114 are shown with genotypes from chromosome 3q marker loci. The distances between adjacent loci are indicated. Homozygous segments are indicated by gray boxes. All of the affected persons show segments of homozygosity within this interval; however, only one marker (D3S1314) is homozygous in all of these individuals, suggesting a location of the disease gene between loci *539-5* and *D3S1288*. (**D**) Overlapping BAC clones spanning the interval containing the disease gene (*13*). The locations of STSs and polymorphic loci are indicated at the top. The location of the disease locus inferred from genetic studies is indicated.

tion, PCLN-1 has a consensus Thr-X-Val PDZ-binding domain at the COOH-terminus (*18*). Although the intracytoplasmic NH_2-termini of the claudins are only six or seven amino acids in length, *PCLN-1* encodes a cytoplasmic NH_2-terminus of 73 amino acids. This segment is highly hydrophilic with a net positive charge. Interestingly, *PCLN-1* encodes a methionine with a suitable Kozak consensus sequence at the position analogous to the start site of other claudins; it is not yet known which of these alternative translation initiation sites is used in vivo. Northern (RNA) blots revealed that *PCLN-1* is expressed as a 3.5-kb transcript that is found only in kidney (Fig. 2C) (*19*). Analysis of genomic organization indicated that *PCLN-1* consists of five exons, each flanked by canonical splice donor and acceptor sequences (Fig. 2D) (*20*).

To determine whether mutations in *PCLN-1* cause renal hypomagnesemia, we screened the coding region and intron-exon junctions for variants and then sequenced the variants (*21*). We identified 10 different mutations that alter the protein in 10 kindreds (Fig. 3). Patients were homozygous for mutations in eight kindreds and compound heterozygotes in two outbred kindreds. The mutations cosegregated with the disease, and none were identified in 160 control chromosomes. Mutations included premature termination as well as splice site and nonconservative missense mutations. For example, affected members of kindred K114 are homozygous for a premature termination codon at position 149, resulting in a protein missing the last three transmembrane domains (Fig. 3A). Similarly, apparently unrelated patients K118-1 and K119-1 both have a homozygous missense mutation substituting arginine for gly-

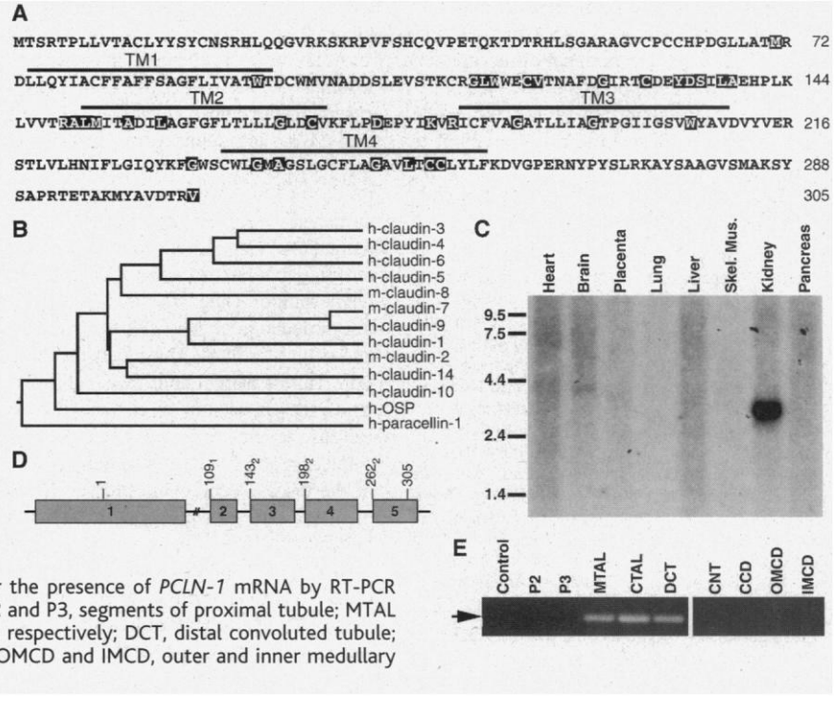

Fig. 2. Sequence, structure, and expression of PCLN-1. (**A**) The deduced amino acid sequence of PCLN-1. Locations of putative transmembrane domains are indicated as TM1 to TM4. Amino acids that are identical to highly conserved residues among claudin family members are highlighted (*11*, *29*). (**B**) Dendrogram of members of the claudin family, whose relationships were determined using the MegAlign Clustal method (*15*) (h, human; m, mouse; OSP, oligodendrocyte-specific protein). (**C**) Northern blot of *PCLN-1*. An autoradiogram of *PCLN-1* hybridized to polyadenylated [poly(A)$^+$] RNA from indicated human tissues is shown; locations of size standards in kilobases are indicated (*19*). Skel. Mus., skeletal muscle; other tissues showing no detectable expression were spleen, thymus, prostate, testis, ovary, small intestine, colon, and peripheral blood leukocyte. (**D**) Genomic organization of the *PCLN-1* gene. The PCLN-1 protein is encoded in five exons (gray boxes). The codon at the beginning of each exon is indicated, and the base within the codon is denoted by the subscript. (**E**) Localization of *PCLN-1* to specific nephron segments. Rabbit nephron segments were microdissected and tested for the presence of *PCLN-1* mRNA by RT-PCR (*22*). The products were fractionated on agarose gel. P2 and P3, segments of proximal tubule; MTAL and CTAL, medullary and cortical thick ascending limb, respectively; DCT, distal convoluted tubule; CNT, connecting tubule; CCD, cortical collecting duct; OMCD and IMCD, outer and inner medullary collecting duct, respectively.

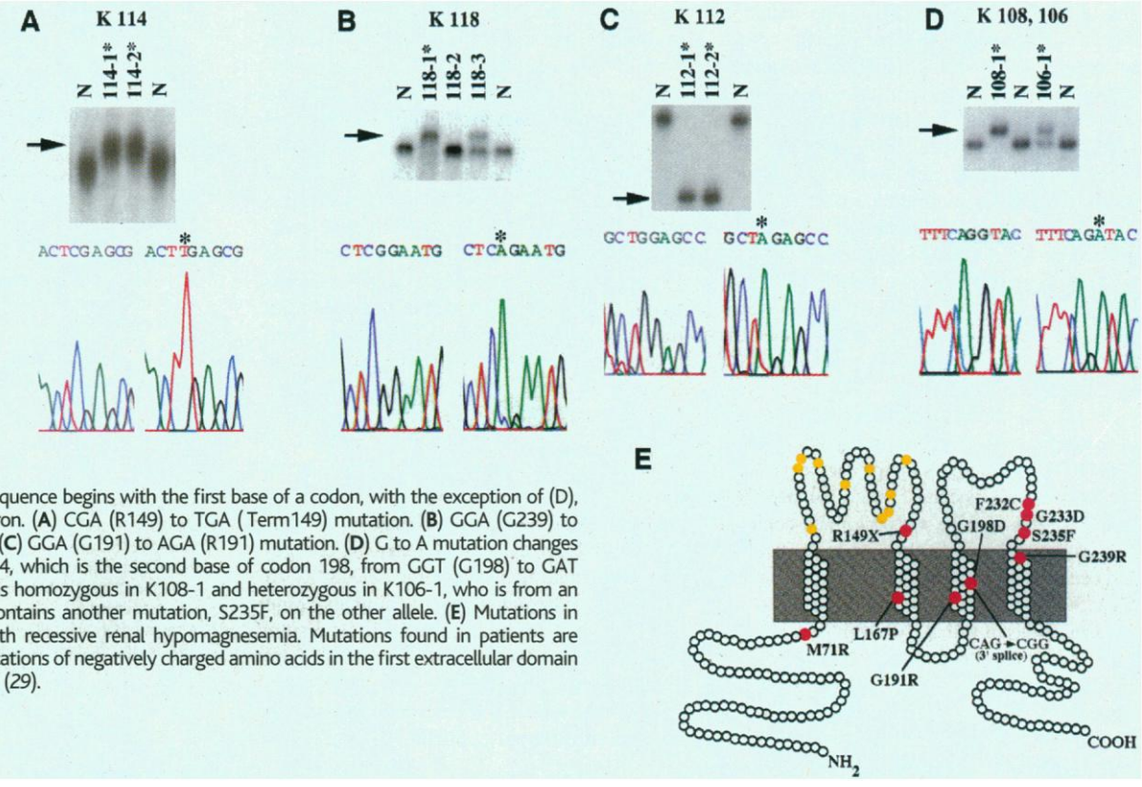

Fig. 3. Mutations in *PCLN-1* in recessive renal hypomagnesemia kindreds. *PCLN-1* variants were identified by SSCP and sequenced (*21*). Autoradiograms are shown at the top of each panel. Affected persons are denoted by an asterisk; unrelated normal persons are denoted by N. Variants are indicated by arrows. Below, the corresponding DNA sequences of the sense strand of wild-type (left) and mutant alleles (right) are shown; mutations are indicated by asterisks. Each sequence begins with the first base of a codon, with the exception of (D), which begins in an intron. (**A**) CGA (R149) to TGA (Term149) mutation. (**B**) GGA (G239) to AGA (R239) mutation. (**C**) GGA (G191) to AGA (R191) mutation. (**D**) G to A mutation changes the first base of exon 4, which is the second base of codon 198, from GGT (G198) to GAT (D198). The mutation is homozygous in K108-1 and heterozygous in K106-1, who is from an outbred kindred and contains another mutation, S235F, on the other allele. (**E**) Mutations in PCLN-1 in patients with recessive renal hypomagnesemia. Mutations found in patients are indicated in red. The locations of negatively charged amino acids in the first extracellular domain are indicated in yellow (*29*).

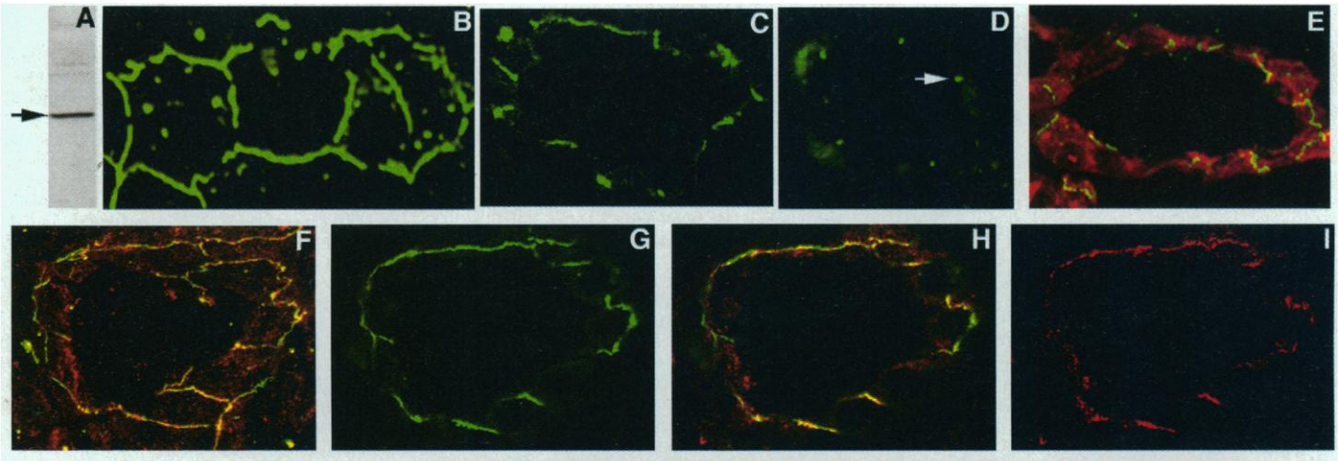

Fig. 4. Immunolocalization of PCLN-1. (**A**) Protein immunoblot of bacteria expressing PCLN-1 probed with anti–PCLN-1 (*23*). A specific band with an apparent molecular mass of 36 kD (arrow) is detected. The remaining panels show immunolocalization of PCLN-1 in frozen human kidney sections. Sections were stained with the indicated antibodies and subjected to confocal microscopy (*24*). Magnifications, ×630. (**B**) Three cells in longitudinal section of renal tubule stained with anti–PCLN-1, showing staining of intercellular junctions. (**C**) Tangential section of tubule stained with anti–PCLN-1, showing staining of intercellular junctions. (**D**) Cross section of tubule stained with anti–PCLN-1, showing localization to apical intercellular junctions (arrow indicates one junction). Each of these junctions costains with anti-occludin (*30*). (**E**) Tangential section of tubule stained with indocarbocyanine (CY3)–labeled anti–Tamm-Horsfall protein (a TAL marker) and fluorescein isothiocyanate (FITC)–labeled anti–PCLN-1. All THP-positive tubules also stain for PCLN-1. The remaining images show colocalization of occludin (FITC-labeled) and PCLN-1 (CY3-labeled) in renal tubules. (**F**) Composite of 36 confocal images demonstrating colocalization (yellow) of occludin and PCLN-1 in intercellular junctions. (**G** to **I**) A single confocal section from (F), showing staining for occludin (G), PCLN-1 (I), and the two superimposed (H), demonstrating colocalization. (**J** to **L**) Individual tubule cell showing staining for occludin (J), PCLN-1 (L), and the two superimposed (K). (**M** to **O**) A vertical section through intercellular junctions shown in (J) to (L) composed of 93 confocal sections (in *z* axis), showing staining for occludin (M), PCLN-1 (O), and the two superimposed (N), confirming colocalization throughout the junction.

cine at codon 239 (Fig. 3B). This mutation introduces a charged residue into the fourth transmembrane domain, replacing the normal glycine residue that is conserved among all members of the claudin family (*11, 17*). The $Gly^{191} \rightarrow Arg$ mutation in K112 (Fig. 3C) alters another completely conserved glycine in the third transmembrane domain.

We next determined where PCLN-1 is expressed in the kidney. Using microdissected nephron segments (*22*), we detected *PCLN-1* mRNA only in TAL and the distal convoluted tubule (DCT) (Fig. 2E). PCLN-1 protein was next localized in kidney sections with the use of an antibody to PCLN-1 (anti–PCLN-1) (Fig. 4A) (*23*). The protein was detected at intercellular junctions of a subset of renal tubules (Fig. 4, B to D), including all tubule segments staining for the TAL-specific Tamm-Horsfall protein (Fig. 4E). Finally, we performed confocal microscopy using antibodies to both PCLN-1 and occludin, a ubiquitous tight junction protein (*24*). PCLN-1 and occludin were found to colocalize, indicating that PCLN-1 is a component of the tight junction (Fig. 4, F to O).

These results identify PCLN-1 as a renal tight junction protein that when mutated causes massive renal magnesium wasting with hypomagnesemia and hypercalciuria, resulting in nephrocalcinosis and renal failure. We infer that these mutations cause loss of normal PCLN-1 function, and that no other genes are redundant in function to *PCLN-1*.

Despite its critical role in many biological functions, the mechanisms underlying Mg^{2+} homeostasis have remained obscure. Genetic studies are now providing new insight into homeostatic determinants. In addition to *PCLN-1*, mutations in the gene encoding the Na^+-Cl^- cotransporter of the DCT have been shown to indirectly cause hypomagnesemia (*25*). Although the mechanism of Mg^{2+} resorption in the DCT is uncertain, it is of interest that *PCLN-1* mRNA is expressed at this site. In addition, two other genes altering either intestinal or renal Mg^{2+} handling have been mapped but not yet identified (*26*).

Our results suggest that PCLN-1 is required for a selective paracellular conductance. We propose that PCLN-1, alone or in partnership with other constituents, forms an intercellular pore permitting paracellular passage of Mg^{2+} and Ca^{2+} down their electrochemical gradients. The existence of such pores was predicted from prior physiologic studies characterizing paracellular conductances (*27*). Such a conclusion is supported by PCLN-1's similarity to claudins, which form intercellular bridges in tight junctions; the location of PCLN-1 in tight junctions of the TAL; the phenotype of patients with mutations in this gene; and the prior physiology implicating the paracellular pathway of the TAL in Mg^{2+} homeostasis. The hypercalciuria seen in patients with mutations is consistent with physiologic evidence that the paracellular pathway of the TAL mediates resorption of both Mg^{2+} and Ca^{2+}. The lesser dependence of Ca^{2+} homeostasis on this paracellular pathway, as well as the ability of parathyroid hormone to increase intestinal absorption and renal transcellular resorption of Ca^{2+}, may account for patients' maintenance of normal serum Ca^{2+} (*28*). Alternatively, given physiologic evidence that this paracellular pathway is regulated by Mg^{2+} concentration, PCLN-1 could be a sensor of Mg^{2+} concentration that alters a paracellular permeability mediated by other factors. PCLN-1 could conceivably mediate both functions, because tight junctions are in contact with fluid on both sides of epithelial layers. It is noteworthy that the first extracellular domain of PCLN-1 is by far the most negatively charged of the claudin family, with 10 negatively charged residues and a net charge of −5 (Fig. 3E). This high density of negative charges may contribute to the cationic selectivity of this paracellular pathway and could also bind Mg^{2+} or Ca^{2+} (or both). Finally, these results raise the possibility that other members of the claudin family also mediate specific paracellular conductances and determine the permeabilities of different epithelia.

References and Notes

1. R. Bonnet, *Dtsch. Med. Wochenschr.* **21**, 58 (1895); M. G. Farquhar and G. E. Palade, *J. Cell Biol.* **17**, 375 (1963); J. M. Anderson and C. M. Van Itallie, *Am. J. Physiol.* **32**, G467 (1995).
2. J. L. Madara, *Annu. Rev. Physiol.* **60**, 143 (1998).
3. L. L. Mitic and J. M. Anderson, *ibid.*, p. 121.
4. G. R. Shareghi and Z. S. Agus, *J. Clin. Invest.* **69**, 759 (1982); A. Di Stefano, N. Roinel, C. De Rouffignac, M. Wittner, *Renal Physiol. Biochem.* **16**, 157 (1993); C. De Rouffignac and G. Quamme, *Physiol. Rev.* **74**, 305 (1994).
5. M. G. Brunette, N. Vigneault, S. Carriere, *Am. J. Physiol.* **227**, 891 (1974); E. Kelepouris and Z. S. Agus, *Sem. Nephrol.* **18**, 58 (1998).
6. G. Quamme and J. H. Dirks, *Am. J. Physiol.* **238**, F187 (1980).
7. T. H. Steele, S. F. Wen, M. A. Evenson, R. E. Rieselbach, *J. Lab. Clin. Med.* **71**, 455 (1968).
8. J. P. Kokko, *Fed. Proc.* **33**, 25 (1974).
9. M. Praga *et al.*, *Kidney Int.* **47**, 1419 (1995). This disease is number 248250 in the Online Mendelian Inheritance in Man (OMIM) database.
10. Kindreds with recessive renal hypomagnesemia were recruited via ascertainment of affected index cases. Genomic DNA was prepared from venous blood of kindred members. The study was performed with approval of the Yale Human Investigation Committee.
11. Additional data are available at www.sciencemag.org/feature/data/1041171.shl.
12. Genotyping was performed by polymerase chain reaction (PCR) using di- and tetranucleotide repeat polymorphisms. Analysis of linkage was performed by homozygosity mapping using the Genehunter program. The trait locus was specified as autosomal recessive with a mutant allele frequency of 0.002, 99% penetrance, and a phenocopy rate of 1%.
13. BAC clones were selected from the RPCI 11 library by hybridization to STSs and their sizes determined by pulse-field gel electrophoresis. BAC ends were sequenced and overlaps of BAC clones were determined by STS content. Locus *539-5*, a dinucleotide repeat with 85% heterozygosity, was identified on BAC 4053-6 (*11*).
14. Exon trapping was performed by subcloning BACs into the vector pSPL3 (Gibco-BRL), transfection into COS-7 cells, and isolation of spliced products, which were cloned and sequenced. This identified exon 3 of PCLN-1, and the complete ORF (GenBank accession number AF152101) was determined by selecting overlapping clones from a human kidney cDNA library. The deduced sequence was confirmed using specific primers to direct PCR from first-strand cDNA derived from human kidney.
15. Analysis of hydrophobicity and sequence similarity was performed using Protean-Kyte-Doolittle hydropathy plot and Megalign Clustal method software, respectively (DNAStar).
16. K. Morita, M. Furuse, K. Fujimoto, S. Tsukita, *Proc. Natl. Acad. Sci. U.S.A.* **78**, 5759 (1999).
17. M. Furuse, K. Fujita, T. Hiragi, K. Fujimoto, S. Tsukita, *J. Cell Biol.* **141**, 1539 (1998).
18. Z. Songyang *et al.*, *Science* **275**, 73 (1997).
19. Exons 3 to 5 of *PCLN-1* cDNA were hybridized to human multiple-tissue Northern blots (Clontech) following standard protocols. A β-actin control probe was used separately to ensure RNA integrity (Y. Lu, data not shown).
20. The intron-exon boundaries of *PCLN-1* were determined by either amplification of gene segments by PCR or subcloning from BAC clones and sequencing of the products.
21. Variants in *PCLN-1* were identified using single-strand conformation polymorphism (SSCP) with *PCLN-1*–specific primer pairs directing PCR using genomic DNA as a template (*11*). Identified variants were sequenced.
22. A segment of rabbit *PCLN-1* cDNA (amino acids 99 to 192 in the human protein) was amplified from a rabbit kidney cDNA library (Clontech) using human PCLN-1 primers. The DNA sequence of the rabbit segment predicts a protein 90% identical to human PCLN-1. Reverse transcription PCR (RT-PCR) with microdissected rabbit nephron segments was performed as described [H. Velazquez *et al.*, *Kidney Int.* **54**, 464 (1998)], using rabbit-specific *PCLN-1* cDNA primers that lie in adjacent exons. Each segment was independently dissected five times and the results were identical each time, with the exceptions that the DCT was negative once and the cortical collecting duct (CCD) was positive once.
23. The peptide VSMAKSYSAPRTETAKMYAVD (*29*) from the COOH-terminus of PCLN-1 was coupled to keyhole limpet hemocyanin. Rabbits were immunized by successive injections, and serum was harvested. Anti–PCLN-1 was affinity-purified using the immunizing peptide coupled to an iodoacetyl cross-linked agarose column. Antibody specificity was determined by protein immunoblotting of bacterial lysates containing polyhistidine-tagged PCLN-1 in vector pET15b (Novagen). A product with an apparent molecular mass of 36 kD was detected in PCLN-1–containing lysates (but not vector-only lysates) using anti–PCLN-1 or mouse monoclonal anti-polyhistidine but not preimmune serum.
24. M. Furuse *et al.*, *J. Cell Biol.* **123**, 1777 (1993). Sections (5 μm) were cut from frozen human kidney specimens, fixed, and immunostained. Sections were visualized via immunofluorescence and confocal microscopy.
25. D. B. Simon *et al.*, *Nature Genet.* **12**, 24 (1996).
26. R. Y. Walder *et al.*, *Hum. Mol. Genet.* **6**, 1491 (1997); I. C. Meij *et al.*, *Am. J. Hum. Genet.* **64**, 180 (1999).
27. P. Claude, *J. Membr. Biol.* **39**, 219 (1978).
28. P. A. Friedman, *Annu. Rev. Physiol.* **60**, 179 (1998).
29. Abbreviations for the amino acid residues are as follows: A, Ala; C, Cys; D, Asp; E, Giu; F, Phe; G, Gly; H, His; I, Ile; K, Lys; L, Leu; M, Met; N, Asn; P, Pro; Q, Gln; R, Arg; S, Ser; T, Thr; V, Val; W, Trp; and Y, Tyr.
30. K. A. Choate, data not shown.

31. We thank the families studied for their participation; V. Benigno, S. Vittoria, and M. Bianchetti for clinical data; C. Nelson-Williams for management of the DNA database; J. Anderson and P. De Camilli for thoughtful advice; and S. Frankel, S. Floyd, and W. Kim for help with confocal microscopy. Supported in part by NIH grant RO1DK51696. K.A.C. is an investigator of the NIH Medical Scientist Training Program; R.P.L. is an investigator of the Howard Hughes Medical Institute.

22 April 1999; accepted 21 May 1999